Journal of Atmospheric and Solar–Terrestrial Physics 215 (2021) 105558

Contents lists available at ScienceDirect

Journal of Atmospheric and Solar–Terrestrial Physics

journal homepage: www.elsevier.com/locate/jastp

Research paper

A vector theory for forward propagation in a structured ionosphere

C.L. Rino *, C.S. Carrano

Institute for Scientific Research, Boston College, Newton, MA, United States of America

ARTICLE INFO

Keywords:
HF propagation
Inhomogeneous propagation

ABSTRACT

The scalar forward propagation equation, most often with the parabolic approximation, has been used extensively for simulating ionospheric radio propagation. More recently, the formalism has been applied at HF frequencies where external magnetic field effects must be accommodated. This paper presents a generalization of the forward propagation equation to accommodate vector fields with forward-marching integration. The ramifications for characteristic mode identification are explored.

1. Introduction

This paper presents a generalization of the forward-propagation-equation (FPE) method to accommodate propagation in the earth's ionosphere at radio frequencies above 3 MHz. Constitutive relations characterize the interaction of electromagnetic (EM) fields with propagation media. In the HF frequency band (3 to 30 MHz) the ionospheric constitutive relation is a tensor, which depends on the direction and strength of the earth's magnetic field. At higher frequencies the dielectric tensor becomes polarization independent, whereby it can be replaced by a scalar.

The homogeneous wave equation characterizes propagation in a uniform medium. Solutions are summations of characteristic modes. Well known examples include plane waves, cylindrical waves, and spherical waves. However, real-world media are temporally varying and spatially inhomogeneous. Maxwell's equations can be formulated in the time-domain or the temporal frequency domain. The frequency-domain formulation will be used in our development. Spatial inhomogeneities are accommodated by incorporating induced secondary radiation.

Obtaining tractable solutions to the inhomogeneous wave equation is challenging because every point in the propagation space is potentially influenced by every other point. The problem is simplified significantly by replacing the second-order differential equation that governs wave propagation with coupled first-order differential equations that separately characterize forward and backward propagation. Forward propagation refers to the direction from a local source of radiation. Induced propagation in the opposite direction (typically Bragg backscatter) is small enough to be neglected insofar as its effect on forward propagation is concerned.

A complete derivation of the vector FPE will be presented. However, it is instructive to review the underlying concepts. The second-order differential equation that governs propagation in a scalar medium has the form

$$\nabla^2 F + n^2 k^2 F = 0, \tag{1}$$

where F represents an EM field component, $k = 2\pi f/c$ with c the vacuum velocity of light and n the refractive index. An assumed form for the solution leads to a formal factorization of (1) as the product of two first-order differential equations of the form

$$\frac{\partial F^{\pm}}{\partial s} = \Theta_n F \pm ik\Delta n F, \tag{2}$$

where $F = F^+ + F^-$ represents the total field as a summation of two fields propagating in opposite directions. The propagation operator, $\Theta_n F^{\pm}$, advances each spatial Fourier component of the field along the $\pm s$ directions. The refractive index has been separated into a background component, n_0, and a perturbation, Δn. In the factored form $ik\Delta n$ is a phase perturbation. The FPE is obtained by neglecting the backscatter contribution (Flatte, 1986; Levy, 2000; Kuttler, 1999).

The attractive feature of the FPE, as represented by (2) with $F^{\pm}$ replaced by F^+, is the explicit identification of additive propagation and media-interaction contributions. The integration step is bounded by planes perpendicular to the propagation reference direction, although the boundaries are not associated with physical layers. Split-step integration applies the media-interaction and propagation terms separately. The integration step starts with a phase perturbation, formally the solution to (2) with $\Theta_n F^+ = 0$. Propagation of the modified field over the distance between the boundary layers completes the integration step.

The scalar FPE, most often with a constraint on the range of propagation angles when it is referred to as the parabolic wave equation (PWE), has been used extensively (W.Kiang and Liu, 1985; Wagen and

* Corresponding author.
E-mail address: crino@bc.edu (C.L. Rino).

https://doi.org/10.1016/j.jastp.2021.105558
Received 18 September 2020; Received in revised form 16 December 2020; Accepted 21 January 2021
Available online 27 January 2021
1364-6826/

Yeh, 1985; Carrano et al., 2011). The deleterious effects of scintillation on beacon satellite communication, surveillance, and positioning systems have motivated much of the research (Knepp, 2004; Carrano et al., 2012; Jiao et al., 2018). More recently, ionospheric propagation at HF has been analyzed using FPE simulations (Hocke and Igarashi, 2003; Carrano et al., 2020). The simulations include surface reflections and show good agreement with ray tracing.

A complete treatment of HF propagation must include polarization dependence. This has been achieved with numerical simulations that exploited rapidly evolving computation capabilities (Wagen and Yeh, 1985). A time-domain frequency-domain method was demonstrated by Nickisch and M.Franke (1996). A vector PWE solution was demonstrated by Brent et al. (1990). The Brent et al. (1990) solution exploits the separation of propagation and media-interaction contributions. Characteristic modes are not considered explicitly in these analyses. Our development identifies a transition from propagation in uniform media, which supports only two eigenvector modes, to propagation in an inhomogeneous medium, which is unconstrained a priori.

2. The vector FPE

The derivation of the vector FPE draws heavily on material in Chapter 7 of *Waves and Fields in Inhomogeneous Media* (Chew, 1990). However, all the applications follow from the principal result (26). For a first reading Section 2.1 can be skipped.

2.1. FPE development from Maxwell's equations

The following time-harmonic form of Maxwell's equations characterize ionospheric propagation at frequencies above 3 MHz.

$$\nabla \times \mathbf{E} = -i\omega \mathbf{B} \tag{3}$$

$$\nabla \times \mathbf{H} = i\omega \mathbf{D} \tag{4}$$

$$\mathbf{B} = \mu_0 \mathbf{H} \tag{5}$$

$$\mathbf{D} = \epsilon_0 \overline{\epsilon} \cdot \mathbf{E} \tag{6}$$

The fields $\mathbf{D}$ and $\mathbf{B}$ are measured in flux units. The fields $\mathbf{E}$ and $\mathbf{H}$ represent electric and magnetic field intensities, respectively. The terms μ_0 and ϵ_0 are fundamental constants such that

$$c = 1/\sqrt{\mu_0 \epsilon_0} \tag{7}$$

is the vacuum velocity of light. Radio frequency and angular frequency are related as $f = 2\pi\omega$. The dielectric tensor, $\overline{\epsilon}$, is defined as

$$\overline{\epsilon} = \overline{I} + X\overline{\chi}, \tag{8}$$

where $\overline{I}$ is the identity matrix and $X\overline{\chi}$ is the susceptibility matrix, which is written as a product of a spatially varying scalar and a 3×3 tensor. Several seminal textbooks, e.g. Budden (1985), Yeh and Liu (1961), and Davies (1996), present calculations of the susceptibility matrix. The Appendix to this paper summarizes the results together with a procedure for calculating the ordinary (O) and extraordinary (X) characteristic modes that propagate in a uniform anisotropic ionosphere.

The vector wave equation is obtained by eliminating $\mathbf{B}$ and $\mathbf{H}$:

$$\nabla \times \nabla \times \mathbf{E} + \omega^2/c^2 \overline{\epsilon} \mathbf{E} = 0. \tag{9}$$

Applying the identity

$$-\nabla \times \nabla \times \mathbf{E} = \nabla^2 \mathbf{E} - \nabla(\nabla \cdot \mathbf{E}), \tag{10}$$

puts the wave equation in its more familiar form

$$\nabla^2 \mathbf{E} + \omega^2/c^2 \overline{\epsilon} \mathbf{E} = \nabla(\nabla \cdot \mathbf{E}). \tag{11}$$

Whereas $\nabla \cdot \mathbf{D} = \mathbf{0}$ and $\nabla \cdot \mathbf{B} = \mathbf{0}$ follow from (3) and (4), the $\nabla(\nabla \cdot \mathbf{E})$ term is finite but usually neglected on the basis that the structure does not induce steep gradients. In this development we assume that the magnetic field is uniform, whereby the variation of the dielectric tensor is confined to the scalar multiplier X. From the Appendix,

$$X = (\omega_p/\omega)^2, \tag{12}$$

where ω_p is the electron plasma frequency. For propagation calculations the vector homogeneous wave equation is written as

$$\nabla^2 \mathbf{E} + k^2(\overline{I} + X\overline{\chi})\mathbf{E} = 0. \tag{13}$$

To pursue the identification of characteristic modes, we let

$$X = X_0 + \Delta X, \tag{14}$$

where X_0 is spatially invariant. Proceeding formally, the free-space dyadic Green function is used to convert (13) to the equivalent integral representation

$$\begin{aligned}\mathbf{E}(\mathbf{r}) &= \mathbf{E}_0(\mathbf{r}) + k^2 X_0 \overline{\chi} \iiint \mathbf{E}(\mathbf{r}') \\ &\quad \times [\mathbf{I} + (1/k)^2 \nabla\nabla] G(|\mathbf{r} - \mathbf{r}'|) d\mathbf{r}' \\ &\quad + k^2 \overline{\chi} \iiint \Delta X(\mathbf{r}') \mathbf{E}(\mathbf{r}') \\ &\quad \times [\mathbf{I} + (1/k)^2 \nabla\nabla] G(|\mathbf{r} - \mathbf{r}'|) d\mathbf{r}',\end{aligned} \tag{15}$$

where $\mathbf{E}_0(\mathbf{r})$ is a solution to the free-space wave equation, and

$$G(|\mathbf{r} - \mathbf{r}'|) = \frac{\exp\{ik|\mathbf{r} - \mathbf{r}'|\}}{4\pi|\mathbf{r} - \mathbf{r}'|}. \tag{16}$$

To identify the leading terms following the equal sign, we make the following observation. If $\Delta X(\mathbf{r}) = 0$, $\mathbf{E}(\mathbf{r})$ must be a solution to the characteristic equation, namely a superposition of characteristic modes. It follows that

$$\begin{aligned}\mathbf{E}_c(\mathbf{r}) &= \mathbf{E}_0(\mathbf{r}) + k^2 X_0 \overline{\chi} \iiint \mathbf{E}(\mathbf{r}') \\ &\quad \times [\mathbf{I} + (1/k)^2 \nabla\nabla] G(|\mathbf{r} - \mathbf{r}'|) d\mathbf{r}'.\end{aligned} \tag{17}$$

With this equivalence, the development of the vector FPE follows the development of the scalar FPE in Rino and Kruger (2001). The following Weyl decomposition expresses the scalar Green function as a summation of plane waves

$$\begin{aligned}G(|\mathbf{r} - \mathbf{r}'|) &= 2i \iint \frac{\exp\{ikg(\kappa)|z - z'|\}}{kg(\kappa)} \\ &\quad \times \exp\{i\vec{\kappa} \cdot (\vec{\eta} - \vec{\eta}')\} \frac{d\vec{\kappa}}{(2\pi)^2}.\end{aligned} \tag{18}$$

The free-space wave vector is defined as

$$\mathbf{k} = [\vec{\kappa}, g(\kappa)], \tag{19}$$

where

$$\begin{aligned}k_z &= kg(\kappa) \\ g(\kappa) &= \sqrt{1 - (\kappa/k)^2}.\end{aligned} \tag{20}$$

Substituting (17) and (18) into (15) and evaluating the Fourier integrations leads to the following spatial Fourier domain representation:

$$\begin{aligned}\hat{\mathbf{E}}(\vec{\kappa}; z) &= \hat{\mathbf{E}}_c(\vec{\kappa}; z + z') + 2ik[\mathbf{I} - \mathbf{ss}] \\ &\quad \cdot \int \hat{\mathbf{S}}(\vec{\kappa}; z') \frac{\exp\{ikg(\kappa)|z - z'|\}}{g(\kappa)} dz'\end{aligned} \tag{21}$$

where $\hat{\mathbf{S}}(\vec{\kappa}; z)$ is the spatial Fourier transform of the product $\Delta X(\vec{\eta}, z)\overline{\chi}$ $\mathbf{E}(\vec{\eta}, z)$. The forward and backward propagating components can be identified by partitioning the integral over z' to isolate the respective sources:

$$\begin{aligned}\hat{\mathbf{E}}^+(\vec{\kappa}; z) &= \hat{\mathbf{E}}_c(\vec{\kappa}; z + z') + 2ik[\mathbf{I} - \mathbf{ss}] \\ &\quad \cdot \int_{-\infty}^{z} \hat{\mathbf{S}}(\vec{\kappa}; z') \frac{\exp\{ikg(\kappa)(z - z')\}}{g(\kappa)} dz'\end{aligned}$$

$$\hat{\mathbf{E}}^{-}(\vec{\kappa};z) = 2ik[\mathbf{I}-\mathbf{ss}] \cdot \int_z^{\infty} \hat{\mathbf{S}}(\kappa;z')\frac{\exp\{ikg(\kappa)\left(z'-z\right)\}}{g(\kappa)}dz'. \tag{22}$$

Converting the incremental equations to differential form leads to the following coupled differential equations

$$\pm\frac{\partial\hat{\mathbf{E}}^{\pm}(\vec{\kappa};z)}{\partial z} = ik\hat{\Theta}_c\hat{\mathbf{E}}^{\pm}(\vec{\kappa};z) + 2ik[\mathbf{I}-\mathbf{ss}]\cdot\hat{\mathbf{S}}(\vec{\kappa};z)/g(\kappa). \tag{23}$$

The contributions of the integral terms are obtained by direct integration. The characteristic mode propagator will be developed in detail below.

Whereas the FPE formulation is exact except for the neglect of backward propagating waves, transformation to spatial-domain equations requires evaluation of the integral

$$\iint \frac{2ik}{g(\kappa)}[\mathbf{I}-\mathbf{ss}]\cdot\hat{\mathbf{S}}(\vec{\kappa};z)\exp\{i\vec{\kappa}\cdot\vec{\eta}\}\frac{d\vec{\kappa}'}{(2\pi)^2} = k^2\iint S(\vec{\eta}-\vec{\eta})[\mathbf{I}+\frac{1}{k^2}\nabla\nabla]G(|\vec{\eta}-\vec{\eta}'|)d\vec{\eta}' \tag{24}$$

We note that

$$\iint G(|\vec{\eta}-\vec{\eta}'|)d\vec{\eta}' = i/(2k). \tag{25}$$

We assume that the variation of $\mathbf{S}(\vec{\eta}-\vec{\eta}')$ is such that the source term can be taken outside the integral. With this assumption (24) can be replaced with $\simeq i\frac{k}{2}\mathbf{S}(\vec{\eta},z)$. A vector FPE can be written as follows:

$$\frac{\partial\mathbf{E}(\vec{\eta},z)}{\partial z} = \Theta_c\mathbf{E}(\vec{\eta},z) + i\frac{k}{2}\Delta X(\vec{\eta},z)\overline{\chi}\mathbf{E}(\vec{\eta},z). \tag{26}$$

where

$$\Theta_c\mathbf{E}(\vec{\eta},z) = \int\int\hat{\mathbf{E}}(\vec{\kappa},z)\exp\{ikn_0g(\kappa)\Delta z\} \times \exp\{i\vec{\kappa}\cdot\vec{\eta}\}\frac{d\vec{\kappa}}{(2\pi)^2} \tag{27}$$

If $\Delta X(\vec{\eta},z)=0$, the propagation operator characterizes propagation in a homogeneous anisotropic background medium. This is the only case for which $n_0 \neq 1$. We will show that in a structured medium $n_0 = 1$, in which case the c subscript is omitted.

The vector FPE is fully three-dimensional. However, for computational efficiency, the vector FPE will only be considered in its two-dimensional form with $\vec{\eta}$ replaced by y.

2.2. Characteristic mode propagation

From the summary in the Appendix, propagation in a uniform medium is constrained to two characteristic modes. Each characteristic mode has the form

$$\mathbf{E}(y,z) = \hat{\psi}\exp\{ikn_p^Ms_zz\} \times \exp\{ikn_p^Ms_yy\}\vec{\epsilon}^M, \tag{28}$$

where M denotes O or X. The wave vector that formally identifies each spatial Fourier mode is

$$\mathbf{k}n_p^M = \left[0, n_p^M\kappa_y, kn_p^M\sqrt{1-(\kappa_y/k)^2}\right]. \tag{29}$$

It follows from the linearity of the homogeneous vector wave equation that

$$\Theta\mathbf{E}^M(y,z) = \int\hat{\psi}^M(\kappa_y,z_0)\vec{\epsilon}^M(\phi)\exp\{ikn_p^M(\phi)\sqrt{1-(\kappa_y/k)^2}|z-z|\} \times \exp\{in_p^M(\phi)\kappa_yy\}\frac{d\kappa_y}{2\pi}, \tag{30}$$

where ϕ is the angle between the propagation vector and the magnetic field. The variable change, $\mu = \kappa n_p{}^M(\phi)$, will transform the relation to a form than can be evaluated as a Fourier transformation

$$\Theta\mathbf{E}^M(y,z) = \frac{1}{n_p^M}\int\hat{\psi}^M(\mu,z_0)\vec{\epsilon}^M(\phi) \times \exp\{ikn_p^M(\phi)\sqrt{1-(\mu/(n_p^M(\phi)k)^2)}|z-z|\} \times \exp\{i\mu y\}\frac{d\mu}{2\pi}. \tag{31}$$

The eigenvectors have the form

$$\vec{\epsilon}^M(\phi) = \begin{pmatrix} 1 \\ 1/R^M(\phi) \\ Q^M(\phi)\end{pmatrix}. \tag{32}$$

The components are indexed by ϕ because of the way they are computed. The definition of the susceptibility matrix depends only on the direction of the magnetic field. However, the computation of the characteristic modes imposes constraints determined by the propagation vector direction.

By confining the magnetic field and the propagation vector to a common plane, the Appleton–Hartree equations, (A.13), (A.14), and (A.15) define the eigenvectors in terms of a single angle measured from the magnetic field to the propagation vector direction. The relation between propagation vector components and the ϕ angle follows the standard Fourier-transform sampling of y and μ:

$$\mu_n = 2\pi n/(Ndy) \tag{33}$$

$$\cos\phi_n = 2\pi\mu_n^M/(Ndy). \tag{34}$$

2.3. Split-step integration

With $\Delta X(y,z)=0$, (26) characterizes HF propagation in a uniform medium or a medium with y invariant structure that varies slowly with z. However, neither the field interacting with the inhomogeneous structure nor the result, $\Delta X(y,z)\overline{\chi}\mathbf{E}(y,z)$, is constrained to be a superposition of characteristic modes. It follows that the only consistent form of the FPE with ΔX finite is

$$\frac{\partial\mathbf{E}(y,z)}{\partial z} = \Theta\mathbf{E}(y,z) + i\frac{k}{2}\Delta X(y,z)\overline{\chi}\mathbf{E}(y,z). \tag{35}$$

where

$$\Theta\mathbf{E}(y,z) = \int\hat{\mathbf{E}}(\kappa_y;z_0)\exp\{ikg(\kappa_y)\left|z-z_0\right|\} \times \exp\{i\kappa_yy\}\frac{d\kappa_y}{2\pi} \tag{36}$$

If the derivation had started with $X_0 = 0$, this result would follow. To demonstrate consistency we consider the zero magnetic field limit, $X = 1-n_p^2$ and $\overline{\chi} = \overline{I}$. With $n_p \simeq 1-\Delta n_p$, it follows that $\Delta X/2 \simeq \Delta n_p$, which shows that the scalar FPE is a special case of the vector FPE when the external magnetic field effects are negligible. The only constraint on the magnitude of ΔX is that $\Delta X < 1$, which is ensured by operation below the electron plasma critical frequency.

Accepting (35) and (36) as defining relations, the FPE integration cycle is initiated with a computation of the interaction of the field with the structure between two defining planes separated by dz. This is achieved by solving the FPE with the propagation operator neglected:

$$\frac{\partial\mathbf{E}(y,z)}{\partial z} = i\frac{k}{2}\Delta X(y,z)\overline{\chi}\mathbf{E}(y,z), \tag{37}$$

With the diagonal decomposition

$$\overline{\chi} = \overline{V}^{-1}\overline{DV}, \tag{38}$$

which is guaranteed by the structure of $\overline{\chi}$, the media-interaction contribution is reduced to three uncoupled equations,

$$\frac{\partial\overline{V}\mathbf{E}(y,z)}{\partial z} = i\frac{k}{2}\Delta X(y,z)\overline{DV}\mathbf{E}(y,z) \tag{39}$$

The solution is

$$\mathbf{E}_{\chi}(y,z) = \overline{V}^{-1}\exp\{i\frac{k}{2}\Delta X(y,z)\overline{D}\Delta z\}\overline{V}\mathbf{E}(y,z). \tag{40}$$

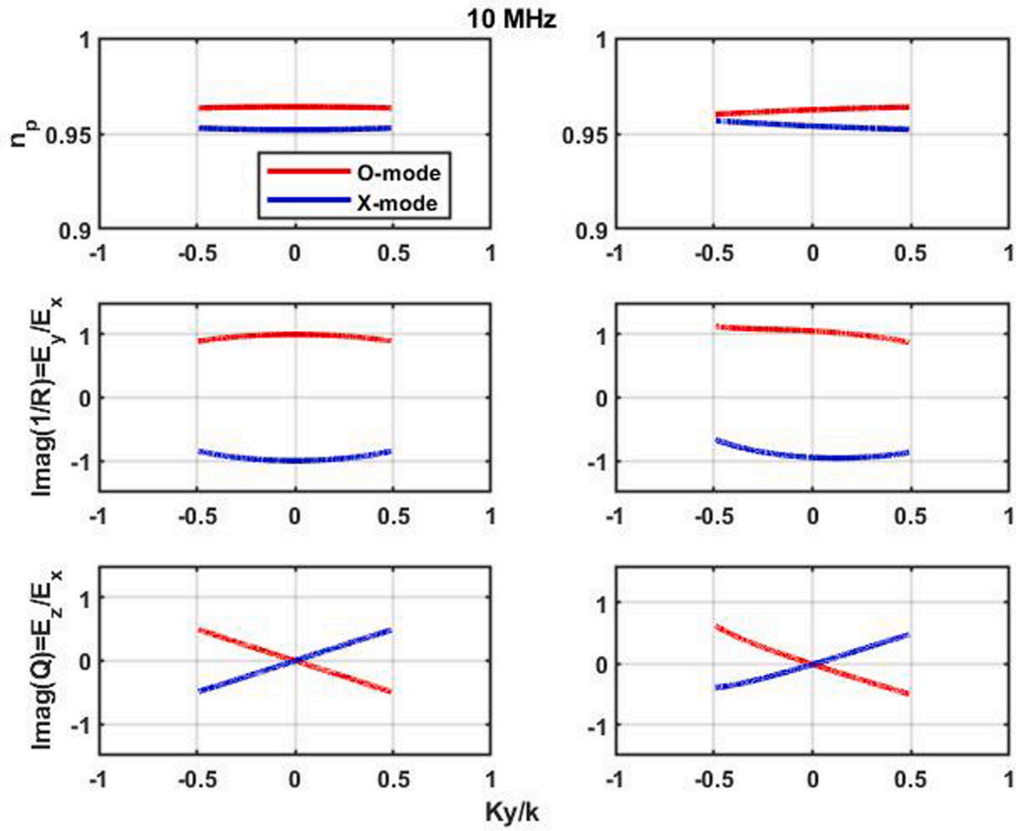

Fig. 1. Eigenvector components versus fractional spatial wavenumber at 10 MHz with $\phi_B = 90°$ (field aligned) and $\phi_B = 45°$. The upper frames shows n_p for each mode. The center and lower frames show the imaginary (non-zero) components of R' and Q, respectively.

The notation $\mathbf{E}_\chi$ distinguishes the field as an intermediate result to be propagated over the distance between the defining z-planes.

The remainder of the paper presents examples illustrating HF vector propagation in uniform, layered, and fully inhomogeneous media.

2.4. Vector FPE simulation examples

A simulation space is defined by the sampled vertical and propagation distances y_n and z_n. The fixed propagation and magnetic field vectors are defined by their polar angles in the xyz system. For two-dimensional simulations both vectors are confined to the yz plane, whereby ϕ_p, ϕ_B are measured from the y axis with $\theta_p = \theta_B = 0$. The defining eigenvector Eqs. (A.13), (A.14), and (A.15) depend on the angles $\phi_n = \phi_{pn} - \pi/2$, which are in turn defined by the spatial wavenumbers

$$\kappa_{yn} = \left(-N_y/2, -N_y/2+1, \ldots, N_y/2-1\right)/(N_y\Delta y)$$
$$\phi_{pn} = \arccos(\kappa_{yn}). \tag{41}$$

Our initial examples are intended to represent boundary-free propagation. Edge effects are suppressed by tapering the fields to zero at the upper and lower boundaries. A 500 km by 300 km data space is used in anticipation of applications to ionospheric propagation over typical HF propagation distances. Plane-wave (modal) illumination is used for scalar simulations. This implies a source at very large distances. For HF simulations a focused beam can be approximated with an appropriate phase distribution.

The first examples illustrate mode-dependent propagation in a uniform background. Fig. 1 summarizes the spatial-frequency-dependent O and X eigenvector components for field-aligned propagation (left frames) and oblique propagation at 45° with respect to the magnetic field (right frames). With broadside field-aligned illumination, the y field components are equal with 90° phase shifts. The z components cancel. These are the conditions for Faraday rotation of the combined linear polarization vector at the Faraday rotation rate

$$FR = k(n_p^O - n_p^X)/2. \tag{42}$$

Changing the magnetic field direction modifies the Faraday rotation mainly by significantly increasing the rotation rate. Increased z sampling was required to resolve the Faraday rotation. The y sampling is dictated by the spatial wavenumber extent of the propagating field components. Because of the lower frequencies the sampling requirements for diffraction are less demanding than higher frequency simulations were polarization effects are negligible.

Fig. 2 shows color displays of the intensities of the combined O and X mode field components for field-aligned (left frame) and oblique(right frame) orientations. One can show that the modulations of the E_x and E_y vary with frequencies equal to twice the Faraday rotation rate and a 90° phase difference. Fig. 3 shows the mode intensity (upper frame) and the measured frequency of the Faraday modulation of the E_y component for the oblique propagation (lower frame). Section 4.5 of Budden (1985) discusses energy propagation in the ionosphere, which involves all three field components. Moreover, the direction of energy propagation need not coincide with the direction of propagation. However, the energy flow is constrained by the incident energy. For this particular example the total polarization field intensity is conserved. Stored energy can reduce the total polarization field intensity. Fully capturing the Faraday frequency is a resolution issue. That is, the propagation steps must resolve the modulation frequency. In Fig. 3 the frequency is slightly underestimated. For the parallel field example $N_y = 8196$ with $N_z = 4096$. For the oblique example $N_z = 16\,384$.

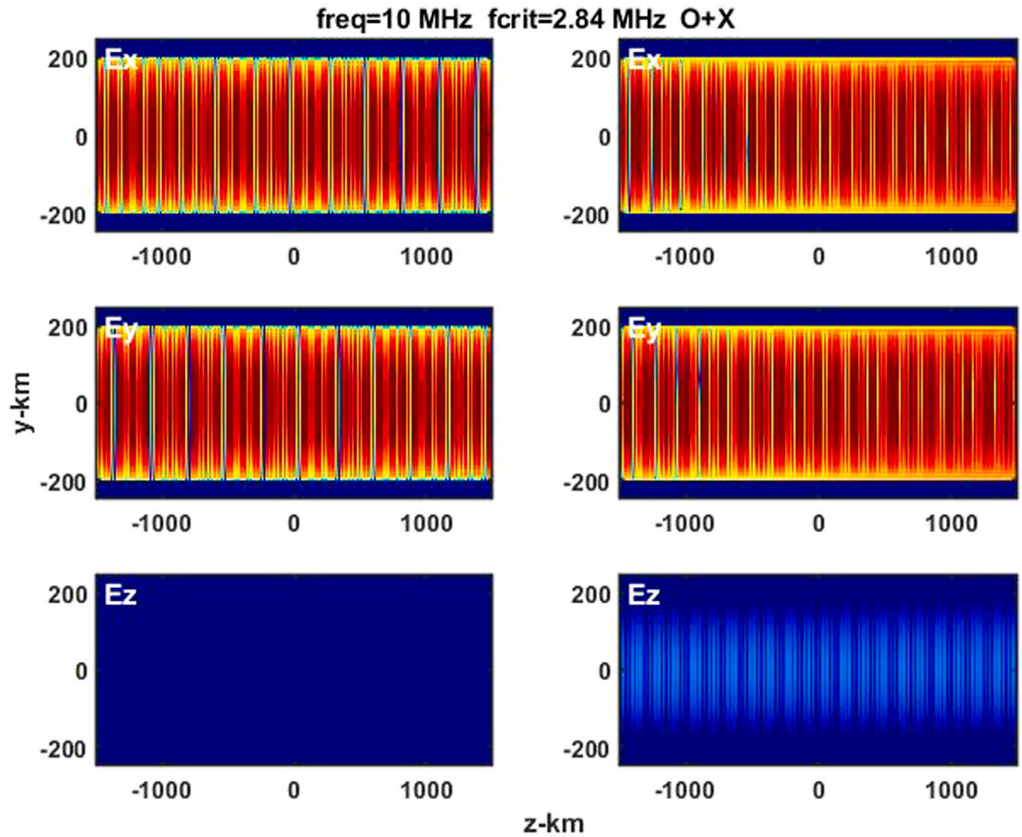

Fig. 2. Color dB intensity displays of E_x (upper), E_y (middle), and E_z (lower) components of the combined mode fields at 10 MHz for the field-aligned (left frames) and oblique geometries (right frames). The displayed range is −40 (dark to light blue) to 0 dB (black to red).

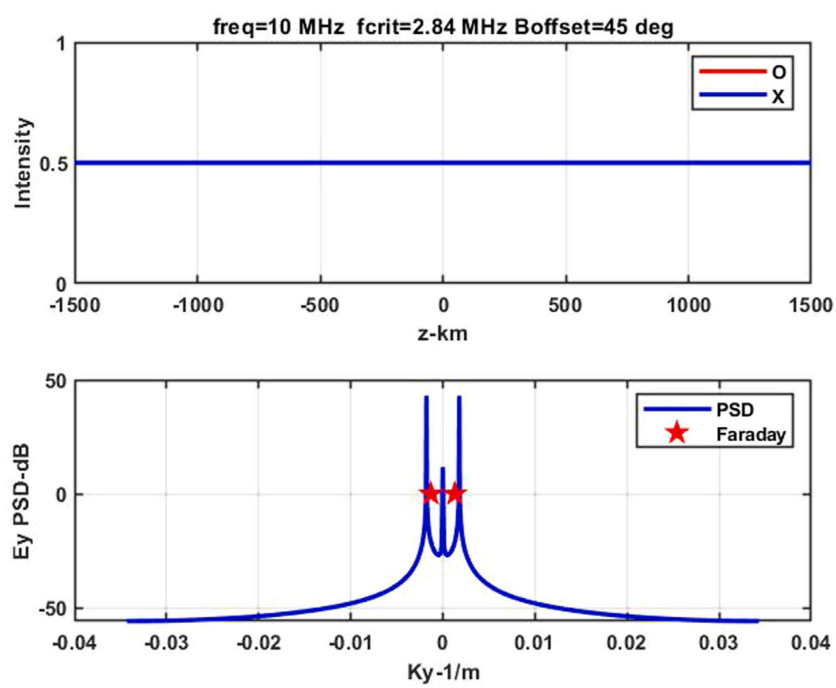

Fig. 3. The upper frame verifies the per mode total field intensity. The lower frame is the periodogram of the combined O and X intensity of the E_y field component for the $\phi_B = 45°$ magnetic field orientation. Red pentagrams show twice the Faraday rate as defined by (42).

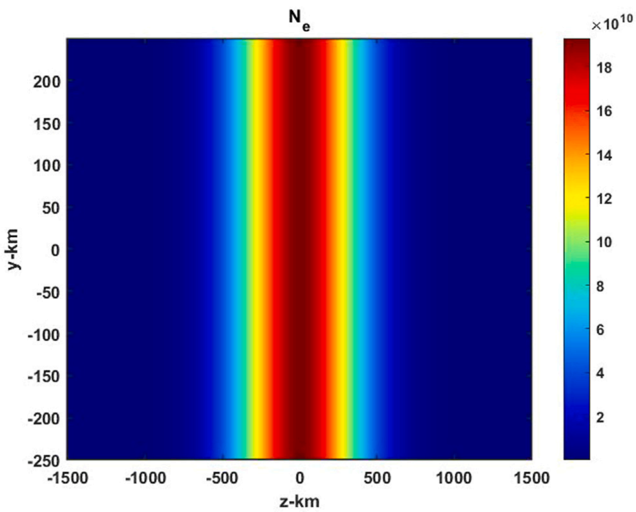

Fig. 4. Electron density ($1/m^3$) with mean z variation.

To introduce varying electron density Fig. 4 shows an environment with a varying mean but no other variation. It is common in such situations to use a layer approximation, which is effectively built into the FPE propagation operator. Fig. 5 shows the variation of the combined field components. The Faraday frequency increases and decreases as expected. Faraday rotation has been used extensively as a diagnostic (Davies, 1980). Knowing the magnetic field direction a measurement of the local Faraday rotation rate can be used to compute the path-integrated electron content. The example illustrates the principle. No attempt was made to extract the path-integrated intensity.

Fig. 6 shows a two-dimensional gaussian density variation. The varying mean electron density variation used in the previous example was derived by integrating the density variation shown in Fig. 6 over y. Structure contributing to each integration step is uniform. However, at each integration step the locally uniform structure was allowed to vary from step to step. The current example is the first vector FPE application that incorporates the media interaction term.

Fig. 7 shows the vector FPE computation of the field components. Whereas the field components shown in Fig. 7 are computed directly, the results shown in Fig. 5 are summations of independently propagated characteristic modes. The gaussian enhancement acts as a divergent lens, which expands the beam. The large E_z component generated by the vector field interacting with $\Delta X(y,z)\overline{\chi}\mathbf{E}(y,z)$ does not directly affect the $\mathbf{E}\times\mathbf{H}$ time-averaged Poynting flux, which is conserved in the calculation, less the energy that is removed by the field taper. Polarization as defined by the E_x and E_y field components is very similar to the polarization generated by combining independently propagating O and X modes, which might be expected because the $\overline{\chi}$ is central to the computation of the characteristic modes.

Fig. 8 shows a Chapman layer, which has been adjusted to refract the upward propagating beam at 10 MHz. The absorbing surface boundary layer is retained to emphasize the vector FPE solution. Surface reflections and propagation over representative earth boundaries will be treated in a separate paper. Fig. 9 shows the progression of the field components. The appearance of a finite E_z component, the modulation of the field component intensities, and the splitting of the refracted beam are caused by the background magnetic field. This is illustrated in Fig. 10, which shows the same simulation with the magnetic field set equal to zero. The two identical field components would be obtained with the scalar FPE.

We expect the structure induced by the magnetic field to be comprised of two near circularly polarized components. Circularly polarized components can be isolated with appropriate combinations of the observable E_x and E_y field components. The simulations are performed in a rectangular coordinate system representative of horizontal and vertical field measurements. The refracted fields are propagating at comparatively small incidence angles, which are exaggerated in the displays. Thus, we expect linear combinations of the simulated E_x and E_y field components to be representative of polarized refracted beam components.

The simulation was initiated with circular polarization, whereas most HF antenna systems transmit linear horizontal or vertical polarization. The only impact this has on measured field components

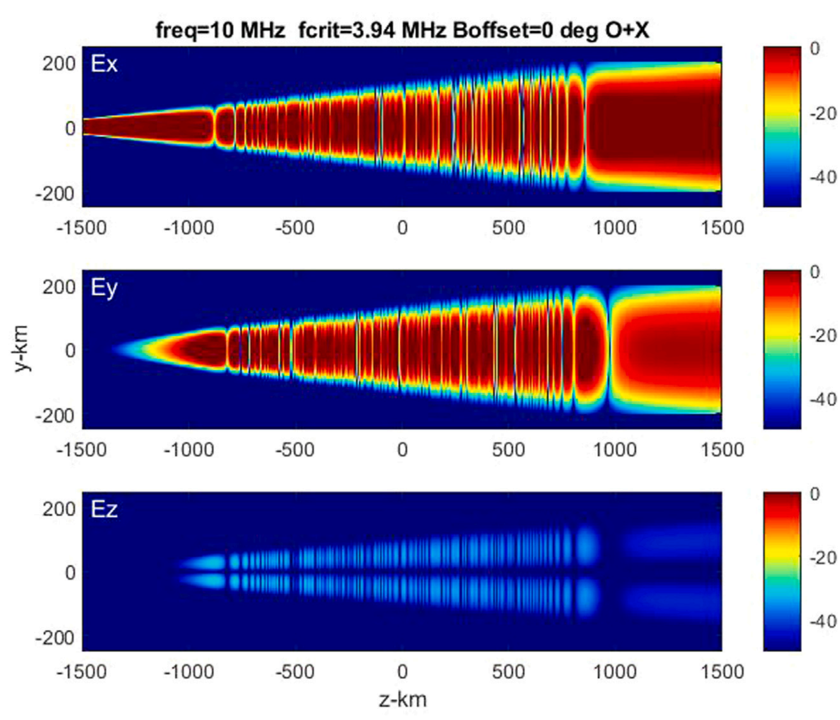

Fig. 5. Color intensity displays of E_x, E_y, and E_z components of the combined mode fields for the simulation space shown in Fig. 4.

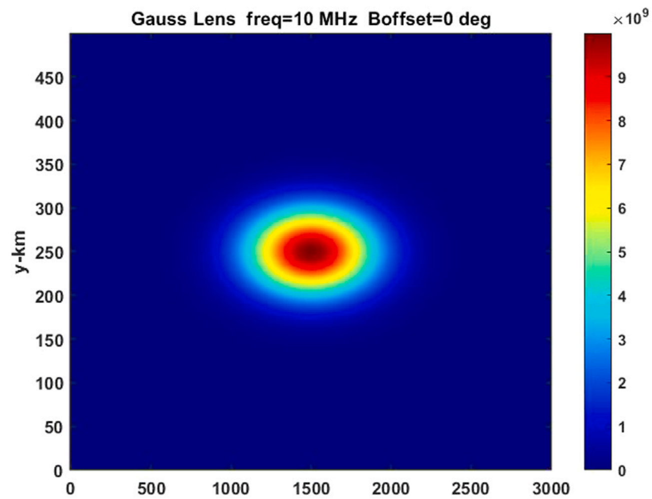

Fig. 6. Color display of a gaussian $N_e(y,z)$ $(1/m^3)$ variation.

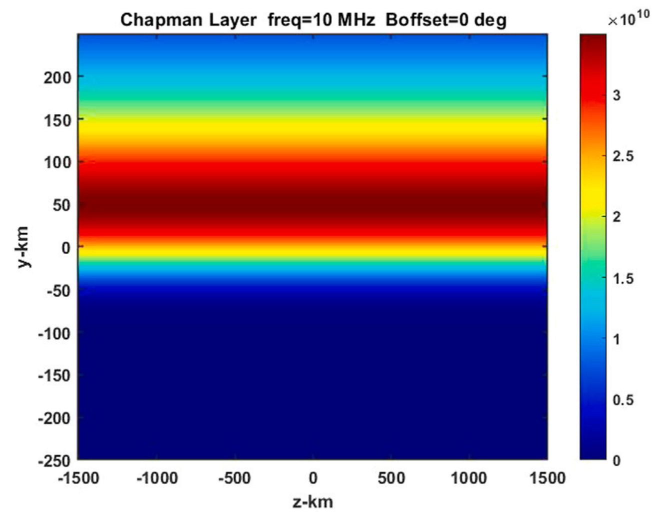

Fig. 8. Chapman layer variation for oblique upward propagation.

is phase reversals. If circular polarization is transmitted, adding and subtracting the measured field components should isolate circularly polarized components. If linear polarization is transmitted, adding and subtracting measured field components with phase reversals produces the same result. Fig. 11 shows the intensity of the added (upper frame) and subtracted (lower frame) field intensities. The modes are isolated with the intensity modulation almost entirely removed.

3. Summary and future applications

The main purpose of this paper was to develop a vector FPE for HF propagation and demonstrate a split-step solution. We found that two versions of the FPE were needed to accommodate propagation in anisotropic media fully. Under conditions of strict homogeneity, only linear combinations of ordinary and extraordinary modes are supported. Summations of characteristic modes are also supported in two-dimensional media with no variation perpendicular to the propagation direction (Fig. 5). For unconstrained inhomogeneous structure there is no prior constraint on the perturbation fields induced by the dielectric tensor. However, Fermat's principle does constrain evolving field structure. We demonstrated that unconstrained FPE solutions to the classic problem of HF refraction by an ionospheric layer generates circularly polarized components that retain the characteristics of ordinary and extraordinary modes.

The results are encouraging, particularly in light of computational efficiency. All results show in this paper can be reproduced in minutes with high-end personal computers. Sampling adequacy can be verified with straightforward consistency checks. Moreover, the results are readily extended to accommodate curved earth, reflecting boundaries,

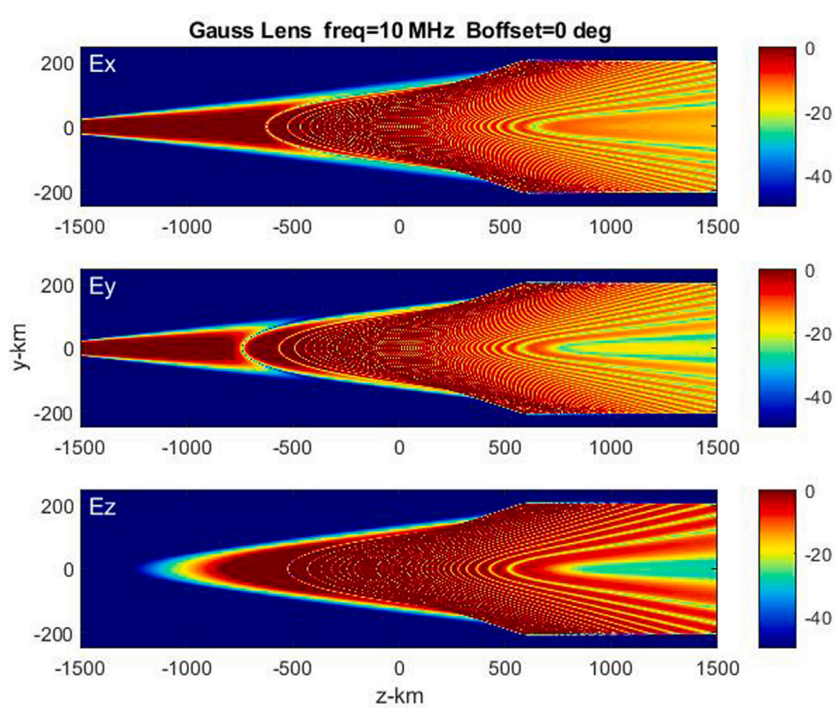

Fig. 7. Color intensity displays of E_x, E_y, and E_z components of the FPE split-step propagation the electron density profile shown in Fig. 6.

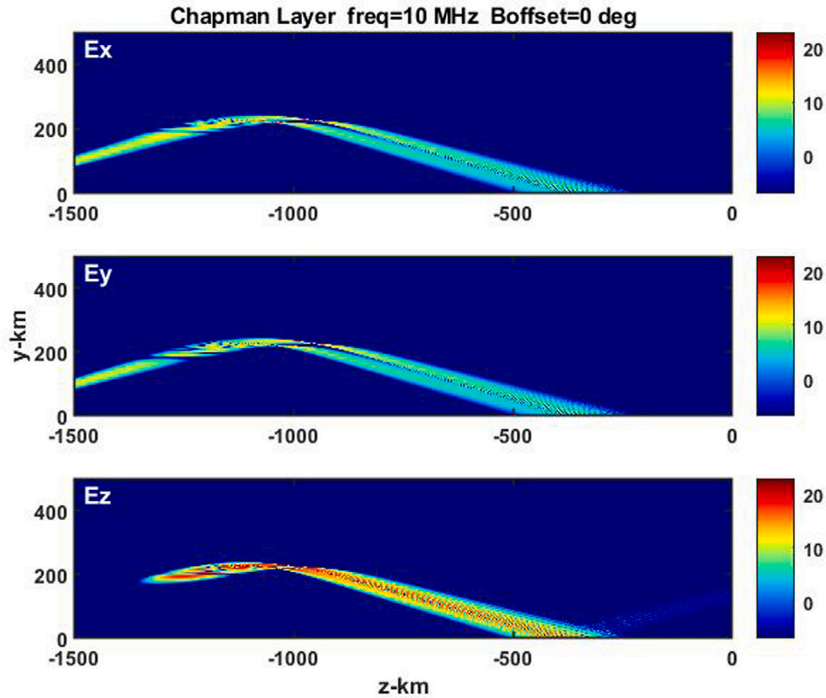

Fig. 9. Color intensity displays of E_x, E_y, and E_z refracted by Chapman layer shown in Fig. 8.

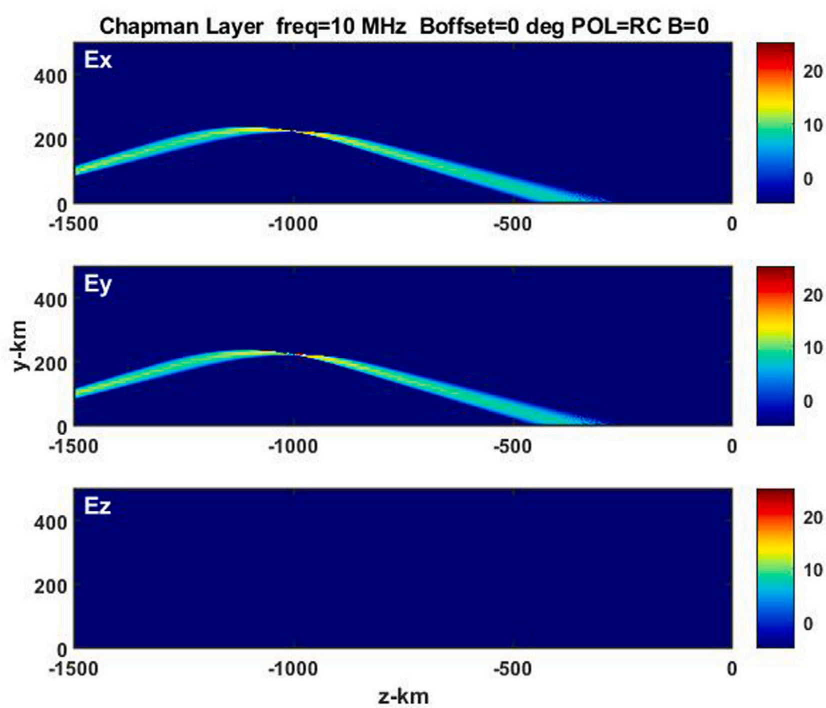

Fig. 10. Color intensity displays of E_x, E_y, and E_z refracted by Chapman layer with zero magnetic field shown in Fig. 8.

and ionospheric structure. We believe the three-dimensional development to be rigorous, but approximations were introduced to implement split-step solutions. Comparisons of the simulations with standard HF analysis procedures for layered media and ray tracing will be pursued.

Acknowledgments

This work was supported by U. S. Air Force Office of Scientific Research under Contract FA8650-20-C-1950. All the results shown in the paper can be reproduced by implementing the FPE as summarized in algorithmic form.

Appendix. Susceptibility matrix and characteristic modes

The susceptibility tensor as defined Equation (4.5.11) of Yeh and Liu (1961) can be written as $X\overline{\chi}$ where

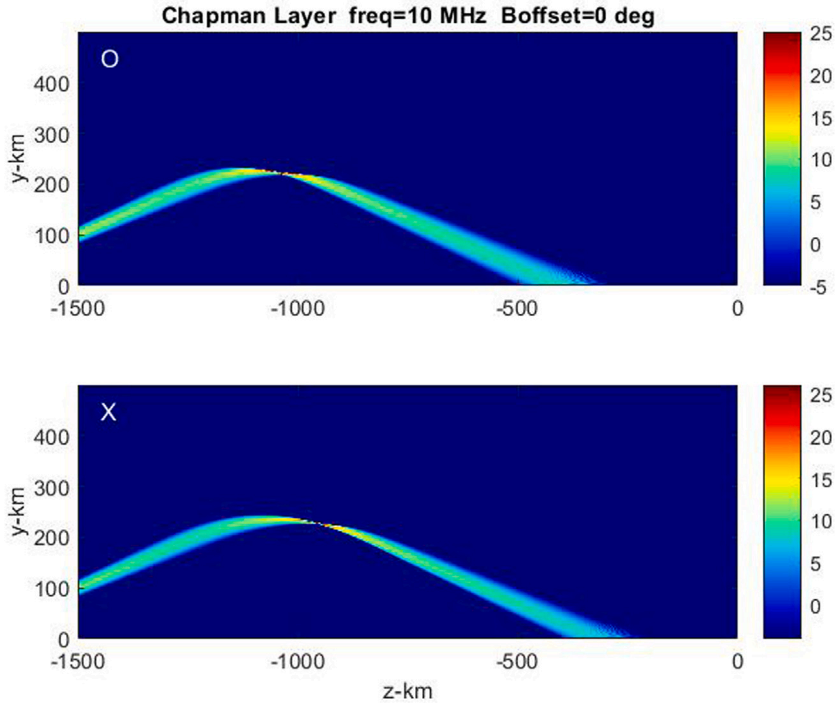

Fig. 11. Color intensity displays of $E_x + E_y$ intensity (upper frame) and $E_x - E_y$ field components (lower frame).

$$\overline{\chi} = -\frac{1}{1-Y^2} \times \begin{bmatrix} 1-Y_x^2 & -Y_xY_y + iY_z & -Y_xY_z - i_y \\ -Y_xY_y - iY_z & 1-Y_y^2 & -Y_yY_z + iY_x \\ -Y_xY_z + iY_y & -Y_yY_z - iY_x & 1-Y_z^2 \end{bmatrix}, \tag{A.1}$$

and

$$X = \omega_p^2/\omega^2 \tag{A.2}$$

$$\mathbf{Y} = \boldsymbol{\omega}_B/\omega \tag{A.3}$$

$$\omega_p^2 = N_e^2/\left(m_e\epsilon_0\right) \text{ Plasma frequency} \tag{A.4}$$

$$\boldsymbol{\omega}_B = -(e/m_e)\mathbf{B}_0 \text{ Gyro frequency.} \tag{A.5}$$

For completeness

$$\begin{aligned} X &= \omega_p^2/\omega^2 \\ &= 4\pi N_e r_e/k^2 \\ r_e &= \frac{1}{4\pi\epsilon_0}\frac{e^2}{m_e c^2}. \end{aligned} \tag{A.6}$$

Aside from fundamental constants, the susceptibility matrix is defined by N_e, ω, and the magnetic field vector

$$\mathbf{B} = B\mathbf{u}_B \tag{A.7}$$

$$\mathbf{u}_B = [\cos\theta_B, \sin\theta_B\cos\phi_B, \sin\theta_B\sin\phi_B]. \tag{A.8}$$

The procedure for calculating the characteristic modes assumes that $\mathbf{E}$, $\mathbf{B}$, and $\mathbf{D}$ vary as $\exp\{i\left(\omega t - kn_p\mathbf{s}\cdot\mathbf{r}\right)\}$. Substituting $\mathbf{E}$, $\mathbf{B}$, and $\mathbf{D}$ into the time-harmonic forms of Maxwell's equations leads to the characteristic equations

$$\begin{aligned} \mathbf{D}\cdot\hat{\mathbf{E}} &= 0 \\ \left[n_p^2\left(\overline{I} - \mathbf{ss}\right) - X\left(\overline{I} + \overline{\chi}\right)\right]\hat{\mathbf{E}} &= 0. \end{aligned} \tag{A.9}$$

The characteristic equation has non trivial solutions if and only if the determinant of the matrix multiplying $\mathbf{E}$ in (A.9) is zero. Upon calculating n_p, the relation $\mathbf{D} = 0$ can be used to calculate the eigenvectors. Alternatively, the eigenvector equations

$$\left[I + X\overline{\chi}^{-1}(\overline{I} - \mathbf{ss})\right]\mathbf{E} = (1/n_p^2)\mathbf{E} \tag{A.10}$$

can be solved directly. Either way, there are only two eigenvectors,

$$\left[1, R^M(\kappa), Q^M(\kappa)\right] \tag{A.11}$$

designated by standard identifiers $M \leftarrow O$ or $M \leftarrow X$. Following the same angle definitions the propagation vector can be written as

$$\mathbf{s} = [\cos\theta_p, \sin\theta_p\cos\phi_p, \sin\theta_p\sin\phi_p]. \tag{A.12}$$

For numerical implementation of vector split-step FPE integration only two-dimensional propagation will be used. This constrains the propagation vector to the yz, plane following our introduction of the z axis as the propagation reference, whereby $\theta_p = \pi/2$. The propagation angle that defines κ is ϕ_p measured from the y axis. Confining the magnetic field to the yz plane supports two-dimensional structure realizations. However, aligning the magnetic field with the x axis also supports two-dimensional realizations.

Choosing the z axis as the propagation reference with no constraint on the direction of the propagation vector is more general. However, significant algebraic simplification is realized by aligning the propagation vector with the z axis. The same simplification is realized for computation of the HF characteristic modes. Following the procedures just described with $\phi_p = \pi/2$ reproduces the Appleton–Hartree equations (4.14.23), (4.14.21), and (4.14.22) in Yeh and Liu (1961):

$$n_p^2(\phi) = 1 - \frac{X}{1 - \frac{Y^2\sin^2(\phi)}{2(1-X)} \pm \left(\frac{Y^4\sin^4(\phi)}{4(1-X)^2} + Y^2\cos^2(\phi)\right)^{1/2}} \tag{A.13}$$

$$\begin{aligned} R(\phi) &= E_x/E_y \\ &= \frac{i}{\cos(\phi)}\left[\frac{Y\sin^2(\phi)}{2(1-X)} \mp \left(\frac{Y^2\sin^4(\phi)}{4(1-X)^2} + \cos^2(\phi)\right)^{1/2}\right] \end{aligned} \tag{A.14}$$

$$\begin{aligned} Q(\phi) &= E_z/E_x \\ &= iY\sin(\phi)(1-n^2)/(1-X) \end{aligned} \tag{A.15}$$

where $\phi = \phi_p - \pi/2$. The field ratios R and Q, and also the vector Y that defines the susceptibility tensor, must be rotated into the computational coordinate system. This rotation is about the x axis by the angle ϕ, which also defines the y wavenumber component.

References

Brent, I., Siegmanna, W.L., Jacobson, M.J., Jacyna, G.M., 1990. Anisotropic electromagnetic wave propagation modeling using parabolic approximations. Radio Sci. 6, 1121–1136.

Budden, K.G., 1985. The Propagation of Radio Waves. Cambridge University Press, Cambridge.

Carrano, C.S., Groves, K.M., Caton, R.G., 2012. The effect of phase scin- tillations on the accuracy of phase screen simulation using deterministic screens derived from GPS and ALTAIR measurements. Radio Sci. 47, http://dx.doi.org/10.1029/2011RS004958.

Carrano, C.S., Groves, K.M., Caton, R.G., Rino, C.L., Straus, P.R., 2011. Multiple phase screen modeling of ionospheric scintillation along radio occulta- tion raypaths. Radio Sci. 46, http://dx.doi.org/10.1029/2010RS004591.

Carrano, C.S., Retterer, J.M., Groves, K.M., Crowley, G., Duly, T.M., Hunton, D.E., 2020. Wave-optics analysis of HF propagation through traveling iono- spheric disturbances and developing plasma bubbles. In: URSI GASS 2020, Rome, Italy, 29 August–5 September 2020.

Chew, W.C., 1990. Waves and Fields in Inhomogeneous Media. A Van Nostrand Renhol.

Davies, K., 1980. Recent progress in satellite radio beacon studies with particular emphasis on the ATS-6 radio beacon experiment. Space Sci. Rev. 25, 357–430.

Davies, K., 1996. Ionospheric Radio Paropagation. Dover Publications.

Flatte, S.M., 1986. The schrodinger equation i classical physics. Am. Assoc. Phys. Teachers 54 (12), 1088–1092. http://dx.doi.org/10.1002/2015RS005903.

Hocke, K., Igarashi, K., 2003. Wave-optical simulation of the oblique hf radio field. Radio Sci. 38 (1039), http://dx.doi.org/10.1029/2002RS002691.

Jiao, Y., Xu, D., Rino, C., Morton, Y., Carrano, C., 2018. A multi-frequency GPS signal strong equatorial ionospheric scintillation simulator: Algorithm performance and characterization. IEEE Trans. Aerospace Electron. Sys. http://dx.doi.org/10.1109/TAES.2018.2805232.

Knepp, D.L., 2004. Effects of ionospheric scintillation on transit satellite measure- ment of total electron content. Radio Sci. 39, http://dx.doi.org/10.1029/2002RS002825.

Kuttler, J., 1999. Differences between the narrow-angle and wide-angle propa- gators in the split-step fourier solution of the parabolic wave equation. Radio Sci. 47 (7), http://dx.doi.org/10.1109/8.785743.

Levy, M., 2000. Parabolic Equation Methods for Electromagnetic Wave Paropagation. The Institution of Electrical Engineers, London.

Nickisch, L.J., M.Franke, P., 1996. Finite difference time domain tests of ran- dom media propagation theory. Radio Sci. 31, 955–963.

Rino, C.L., Kruger, V.R., 2001. A comparison of forward boundary integral and parabolic wave equation propagation models. IEEE Trans Prop. Anten- nas 49.

Wagen, J.F., Yeh, K.C., 1985. Simulation of hf propagation and angle of arrival in a turbulent ionosphere. Radio Sci. 24, 196–208.

W.Kiang, Y., Liu, C.H., 1985. Multiple phase-screen simulation of wave propa- gation in the turbulent stratified ionosphere. Radio Sci. 20, 652–668.

Yeh, K.C., Liu, C.H., 1961. The Theory of Ionospheric Waves. Academic Press, New York.